Polynomial approximations of Poincaré maps for Hamiltonian systems.

Froeschlé C.
Observatoire de Nice, France
claude@obs-nice.fr

Petit J-M.
C.N.R.S., Observatoire de Nice, France
petit@obs-nice.fr

Abstract

Different methods are proposed and tested for transforming a non linear differential system, and more particulary a hamiltonian one, into a map without having to integrate the whole orbit as in the well known Poincaré return map technique. We construct piecewise polynomial maps by coarse-graining the phase surface of section into parallelograms using values of the Poincaré maps at the vertices to define a polynomial approximation within each cell. The numerical experiments are in good agreement with both the real symplectic and Poincaré maps. The agreement is better when the number of vertices and the order of the polynomial fit increase. Computations of Lyapunov Characteristic Exponents give a measure of how well the fit approximate the different maps.

1 Introduction

Poincare return maps are widely used in all fields of non linear dynamics including celestial mechanics (see Hénon 1981). However return maps often require a lot of computer time since it is necessary to integrate the differential equations to plot them. In order to investigate the long-term stability of test particles in the solar system many authors have therefore sought simpler and more tractable equations which approximate at least qualitatively the original newtonian equations. This is the aim of classical perturbation theory which uses canonical transformations of the variables in order to successively push the non integrable part of the hamiltonian to higher and higher orders. Such an approach continued until the implications of Poincaré's theoretical work in this field were fully appreciated in the sixties with the computer revolution (see Hénon 1981). Poincaré showed that most hamiltonian systems do not possess the integrals required to reduce the solution to quadratures and that trajectories near unstable periodic orbits possess extraordinary complexity. Then in order to keep this complexity one has to resort to numerical experiments. Therefore it is important to increase the computing speed. A first attempt was made using numerical averaging which led to an order of magnitude increase in speed. Let us emphasize that this kind of approach,used by Schubart (1968) in the framework of asteroidal resonant motions, differs radically from the so called averaging principle (see Arnold 1976): Schubart does not drop short periodic terms and does not use series expansions. Therefore with Schubart's averaging there is no restriction for eccentricities or resonance type, and chaotic behavior is still present (see Froeschle and Scholl 1981). The next step which drastically increases the speed of the computation is to replace the hamiltonian dynamical system by a symplectic mapping (an area preserving mapping for systems with two degrees of freedom). This programme has been carried out quite successfully to analyze the long-term behavior of asteroids near resonances with Jupiter (see Wisdom 1982, Murray 1986, Sidlichovsky 1986). However the so-called Chirikov- Wisdom method for building such mappings near resonances is not reliable with the same accuracy all over the phase space. The key point is: the truncated secular part of the hamiltonian should be solvable analytically as well as not changing the topology of the phase space too much. Actually the higher the eccentricity becomes the less reliable is the mapping. Therefore even for the 3/1 resonance, (whose shape was brilliantly explained by Wisdom using his mapping), after the first increase of eccentricity the features of the real orbits may be significantly different from those of the mapping orbits. In the same spirit Sagdeev and Zaslavsky (1987) and Petrosky and Broucke (1988) have derived a two dimensional mapping which describes the dynamics of long period cometary motion within the framework of the restricted three body problem. The basic idea is again to separate out an integrable part (the two body motion) valid for large period of time where the comet is far from the "collision zone" (i.e. the zone where Jupiter interacts strongly with the comet) and a collisional part. This collision induces a change in the energy and angular momentum of the comet and this is modelled by taking into account, using Fourier analysis, the fact that the time interval between "collisions" is very large compared with the "collision" duration. Hadjidemetriou (1986) also solved the unperturbed equations and found the corresponding mapping on a surface of section. Then he perturbed the mapping in such a way that some structures of the phase space known through numerical experiments (stability or unstability of some families of periodic orbits for the given example: 3/1 commensurability) was included in the perturbed mapping. Finally, and again in the framework of the restricted three-body problem (Sun-Jupiter-test particle), a mapping has been derived by Duncan, Quinn and Tremaine (1989) in order to study the long term evolution of planetesimal like orbits i.e. orbits with small eccentricities in the solar system. They used the approximation based on the fact that planets have small eccentricities and the fractional difference in semi major axes between the orbit of a test particle which is nearly circular and the nearest planet is small. Then the perturbations to the motion of the test particle are localised near conjunction with the planet and the first-order perturbations to the orbital elements can be computed analytically using Hill's equations (Hénon and Petit 1986) or equivalently Gauss' or Lagrange's equations. Away from conjunction, as for the nearly parabolic case, the perturbing effect of the planet is assumed to be negligible and hence the orbital elements after conjunction remain unchanged until the next conjunction. All these mappings have been devised using the same kind of approach: use of special features of the motion i.e. resonant orbits, near parabolic or near circular orbits. These mappings are reliable as long as one remains within the domain of validity of the approximations, made in order to isolate an integrable part and some instantaneous perturbations. In any case, these mappings are not reliable for close approaches, which are at the origin of the stochastic motion of short-period comets and of Appolo-Amor asteroids (Milani et al 1989). This underlying stochasticity is at the basis of the mappings worked out by Rickman and Vaghi (1976) and Froeschle and Rickman (1980). Within the framework of the elliptic restricted three body problem their mapping consists in regarding the perturbations of the orbital elements for one orbital revolution as a stochastic variable. More precisely, for different cells in phase space, separate distributions of perturbations are calculated. The orbital evolution is then simulated as a sequence of perturbations randomly chosen according to the calculated distribution. The validity of such procedures has been recently studied by Froeschle and Baille (1989) who have shown some drawbacks of the method which may be considered as being valid only from a statistical point of view and again only within some regions of phase space. The point to be emphasized is that even inside regular regions the method introduces a diffusion which has no physical meaning.

All these mappings are ad hoc and are valid only in some regions of phase space and for specific purposes. We wish to build a mapping valid everywhere in phase space following an idea already used by Varosi et al (1987) but in the framework of non hamiltonian systems, i.e. systems where attractors do exist. The method consists of coarse-graining the phase space surface of section and then interpolating the values of the image of a point. In section 2 we present and discuss the different interpolations we have used in addition of the linear one already used by Varosi et al (1987). In section 3 we give the numerical results concerning the different synthetic mappings compared with both the standard map and the Poincare map of the restricted three body problem.

2 The synthetic mappings

The basic idea of the synthetic mapping is to interpolate the image of a point, when given the images of a set of points located at the vertices of a grid. The simplest way to achieve this is to use linear interpolation (Varosi et al, 1987). Unfortunately, this requires a rather fine graining of the phase space, i.e. we have to compute a lot of points on the grid. We shall try to find more accurate methods. The more commonly used methods of higher order are the Taylor and Spline interpolations.

2.1 Taylor interpolation

We know the value of the functions $x^{(n+1)} = f(x^{(n)}, y^{(n)})$ and $y^{(n+1)} = g(x^{(n)}, y^{(n)})$ at discrete points x_i and y_j. The points are equally spaced in x and y. We want to interpolate the values of f and g at any point. We first derive the interpolation formula in one dimension. We write the Taylor expansion for f about a point in the middle of a given interval, $x' = (x_i + x_{i+1})/2$:

$$\begin{aligned} f(x) &= f(x') + (x-x')f'(x') + \frac{(x-x')^2}{2}f''(x') + \frac{(x-x')^3}{6}f'''(x') \\ &+\frac{(x-x')^4}{24}f^{(4)}(x') + \frac{(x-x')^5}{120}f^{(5)}(x') + \mathrm{O}\left((x-x')^6\right). \end{aligned} \tag{1}$$

We use a centered point to insure the symmetry of the formula. We need to know the value of f and its derivatives at x'. For this we write (1) for x_{i-2}, x_{i-1} and x_i:

$$\begin{aligned} f(x_{i-2}) &= f(x') - \frac{5h}{2}f'(x') + \frac{25h^2}{8}f''(x') - \frac{125h^3}{48}f'''(x') \\ &+\frac{625h^4}{384}f^{(4)}(x') - \frac{3125h^5}{3840}f^{(5)}(x') + \mathrm{O}(h^6), \\ f(x_{i-1}) &= f(x') - \frac{3h}{2}f'(x') + \frac{9h^2}{8}f''(x') - \frac{27h^3}{48}f'''(x') \\ &+\frac{81h^4}{384}f^{(4)}(x') - \frac{243h^5}{3840}f^{(5)}(x') + \mathrm{O}(h^6), \\ f(x_i) &= f(x') - \frac{h}{2}f'(x') + \frac{h^2}{8}f''(x') - \frac{h^3}{48}f'''(x') \\ &+\frac{h^4}{384}f^{(4)}(x') - \frac{h^5}{3840}f^{(5)}(x') + \mathrm{O}(h^6), \end{aligned} \tag{2}$$

where $h = x_{i+1} - x_i$. The corresponding formulae for $f(x_{i+1})$, $f(x_{i+2})$ and $f(x_{i+3})$ are obtained from those for $f(x_i)$, $f(x_{i-1})$ and $f(x_{i-2})$ respectively by changing the minus signs into plus signs. Neglecting terms of order 6 or higher, one can inverts (2) and write $f(x')$, $f'(x')$, $f''(x')$, $f'''(x')$, $f^{(4)}(x')$and $f^{(5)}(x')$ as functions of $f(x_{i-2})$, $f(x_{i-1})$, $f(x_i)$, $f(x_{i+1})$, $f(x_{i+2})$ and $f(x_{i+3})$.

$$
\begin{aligned}
f(x') &= \frac{1}{256}[3f(x_{i-2}) - 25f(x_{i-1}) + 150f(x_i) \\
&\quad +150f(x_{i+1}) - 25f(x_{i+2}) + 3f(x_{i+3})], \qquad (3) \\
hf'(x') &= \frac{1}{1920}[-9f(x_{i-2}) + 125f(x_{i-1}) - 2250f(x_i) \\
&\quad +2250f(x_{i+1}) - 125f(x_{i+2}) + 9f(x_{i+3})], \\
h^2 f''(x') &= \frac{1}{48}[-5f(x_{i-2}) + 39f(x_{i-1}) - 34f(x_i) \\
&\quad -34f(x_{i+1}) + 39f(x_{i+2}) - 5f(x_{i+3})], \qquad (4) \\
h^3 f'''(x') &= \frac{1}{8}[f(x_{i-2}) - 13f(x_{i-1}) + 34f(x_i) \\
&\quad -34f(x_{i+1}) + 13f(x_{i+2}) - f(x_{i+3})], \\
h^4 f^{(4)}(x') &= \frac{1}{2}[f(x_{i-2}) - 3f(x_{i-1}) + 2f(x_i) \\
&\quad +2f(x_{i+1}) - 3f(x_{i+2}) + f(x_{i+3})], \\
h^5 f^{(5)}(x') &= [-f(x_{i-2}) + 5f(x_{i-1}) - 10f(x_i) \\
&\quad +10f(x_{i+1}) - 5f(x_{i+2}) + f(x_{i+3})].
\end{aligned}
$$

By substituting into (1), we obtain:

$$
\begin{aligned}
f(x) &= \Phi_{-2}(\frac{x-x'}{h})f(x_{i-2}) + \Phi_{-1}(\frac{x-x'}{h})f(x_{i-1}) \\
&\quad +\Phi_0(\frac{x-x'}{h})f(x_i) + \Phi_1(\frac{x-x'}{h})f(x_{i+1}) \qquad (5) \\
&\quad +\Phi_2(\frac{x-x'}{h})f(x_{i+2}) + \Phi_3(\frac{x-x'}{h})f(x_{i+3}),
\end{aligned}
$$

where the functions $\Phi_n(X)$, $n = -2, -1, 0, 1, 2, 3$ read:

$$
\begin{aligned}
\Phi_{-2}(X) &= \frac{1}{3840}[45 - 18X - 200X^2 \\
&\quad +80X^3 + 80X^4 - 32X^5], \\
\Phi_{-1}(X) &= \frac{1}{3840}[-375 + 250X + 1560X^2 \\
&\quad -1040X^3 - 240X^4 + 160X^5],
\end{aligned}
$$

$$
\begin{aligned}
\Phi_0(X) &= \frac{1}{3840}[2250 - 4500X - 1360X^2 \\
&\quad +2720X^3 + 160X^4 - 320X^5], \\
\Phi_1(X) &= \frac{1}{3840}[2250 + 4500X - 1360X^2 \\
&\quad -2720X^3 + 160X^4 + 320X^5], \\
\Phi_2(X) &= \frac{1}{3840}[-375 - 250X + 1560X^2 \\
&\quad +1040X^3 - 240X^4 - 160X^5], \\
\Phi_3(X) &= \frac{1}{3840}[45 + 18X - 200X^2 \\
&\quad -80X^3 + 80X^4 + 32X^5].
\end{aligned} \tag{6}
$$

To interpolate a two dimensional function, we need an array of 36 values of f. For the 6 different values of y (viz. y_{i-2}, y_{i-1}, y_i, y_{i+1}, y_{i+2} and y_{i+3}), one evaluates the value of f at the given x. Then one uses these values to interpolate along the y-axis.

2.2 Accuracy and cost

The main goal of this work is to accelerate the iterations of a mapping from a Hamiltonian flow. Therefore one of the crucial points for long term iterations is the area preservation. The error in the position of the image of a point is of order 6. Let (x_0, y_0) be the real image and (x, y) the interpolated one. We can write:

$$
x = x_0 + \epsilon_x(x_0, y_0)h^6, \qquad y = y_0 + \epsilon_y(x_0, y_0)h^6. \tag{7}
$$

A small displacement from the interpolated point is related to that from the real image by:

$$
\begin{aligned}
dx &= dx_0 \left[1 + \frac{\partial \epsilon_x}{\partial x} h^6\right] + \frac{\partial \epsilon_x}{\partial y} h^6 dy_0, \\
dy &= dy_0 \left[1 + \frac{\partial \epsilon_y}{\partial y} h^6\right] + \frac{\partial \epsilon_y}{\partial x} h^6 dx_0.
\end{aligned} \tag{8}
$$

Therefore the relative error of the small area is of order 6:

$$
dx.dy = dx_0.dy_0 \left[1 + \mathrm{O}(h^6)\right]. \tag{9}
$$

Futhermore, suppose we are interested in details of size ϵ in the phase portrait. The size of the grid needed to represent such a detail is of order $\epsilon^{1/5}$. For example, to represent a detail of size 0.001, one needs a grid of size 0.25. So one needs to know the real value of the image at only a few points. This is very interesting for hamiltonian flows that are very long to integrate numerically.

But one never gets something from nothing, and one has to pay for this advantage. The cost is the number of operations involved. For a 2D mapping (two dimensional mapping), we first evaluate the six polynomials (6), i.e. 30 multiplications and 30 additions for the x component. Then, we evaluate six times (5) for the six different values of y. And this is repeated for the 2 components of the image. This second step requires 72 multiplications and 60 additions. Then we evaluate the six polynomials (6) for the y component and evaluate (5) for the 2 components of the image. The total cost is 144 multiplications and 130 additions. This is far from negligible. For a four dimensional mapping, the cost increases to 6336 multiplications and 5300 additions.

2.3 Taylor interpolation of order 3

All the above calculations can be done for a lower order approximation, say for a Taylor expansion of order 3. In this case the error is of order h^4. To interpolate we need to know the image of four points for one dimension. The polynomials involved are:

$$\begin{aligned} \Phi_{-1}(X) &= \frac{1}{48}\left[-3 + 2X + 12X^2 - 8X^3\right], \\ \Phi_0(X) &= \frac{1}{48}\left[27 - 54X - 12X^2 + 24X^3\right], \\ \Phi_1(X) &= \frac{1}{48}\left[27 + 54X - 12X^2 - 24X^3\right], \\ \Phi_2(X) &= \frac{1}{48}\left[-3 - 2X + 12X^2 + 8X^3\right]. \end{aligned} \tag{10}$$

This amounts to 64 multiplications and 54 additions for a 2D mapping, and 1408 multiplications and 1068 additions for a 4D one.

2.4 Spline interpolation

The idea underlying the use of a Spline is to represent a curve by a piece-wise polynomial curve which is as smooth as possible. For a Spline of order 3, we use four points and write the interpolated value as a linear combination of the function at those points:

$$\begin{aligned} f(x) &= \Phi_{-1}(\frac{x-x'}{h})f(x_{i-1}) + \Phi_0(\frac{x-x'}{h})f(x_i) \\ &\quad +\Phi_1(\frac{x-x'}{h})f(x_{i+1}) + \Phi_2(\frac{x-x'}{h})f(x_{i+2}), \end{aligned} \tag{11}$$

where functions Φ_i are polynomials of degree 3. Futhermore these polynomials are chosen so that: the resulting functions and their respective first derivative are continuous. This is achieved if:

$$\begin{aligned} f'(x_i) &= \frac{f(x_{i+1}) - f(x_{i-1})}{2h}, \\ f'(x_{i+1}) &= \frac{f(x_{i+2}) - f(x_i)}{2h}, \end{aligned} \tag{12}$$

which implies the following values for the Φ_i's:

$$\begin{array}{rrrr} \Phi_{-1}(0) = 0, & \Phi_{-1}(1) = 0, & \Phi'_{-1}(0) = -0.5, & \Phi'_{-1}(1) = 0, \\ \Phi_0(0) = 1, & \Phi_0(1) = 0, & \Phi'_0(0) = 0, & \Phi'_0(1) = -0.5, \\ \Phi_1(0) = 0, & \Phi_1(1) = 1, & \Phi'_1(0) = 0.5, & \Phi'_1(1) = 0, \\ \Phi_2(0) = 0, & \Phi_2(1) = 0, & \Phi'_2(0) = 0, & \Phi'_2(1) = 0.5. \end{array} \tag{13}$$

Solving these equations, one finally finds:

$$\begin{aligned} \Phi_{-1}(X) &= -0.5X\left(1 - X^2\right), \\ \Phi_0(X) &= (1 - X)\left(1 + X - 1.5X^2\right), \\ \Phi_1(X) &= X\left(0.5 + 2X - 1.5X^2\right), \\ \Phi_2(X) &= -0.5X^2\,(1 - X). \end{aligned} \tag{14}$$

A straightforward calculation shows that this is a second order method, i.e, the error is of order h^3. Despite the continuity of the first derivative, this is worse than the Taylor expansion of order 3, because we are more interested in the accuracy than in the smoothness of the interpolation.

All these schemes use more points than just the vertices of the cell in question. In cases where there is a limit for one variable, these points may fall in a region where the mapping is not defined. Therefore we need asymmetrical formulae to handle the border cells. These formulae are given in Appendix A.

3 Results

Obviously the different synthetic mappings which have been described in section 2, have two key parameters: the number of divisions in each direction $N = (\text{total number of cells})^{(1/D)}$, where D ($D = 2$ in this paper) is the dimension of the surface of section and the order M of the Taylor expansion. In order to explore the validity of the synthetic approach we applied our method to two cases:

1 An algebraic area preserving mapping for which the computation of orbits is very fast. This allows us to calculate a lot of orbits and to perform enough iterations for a meaningful comparison.

2 A special case of the restricted three body problem studied by Duncan et al (1989).

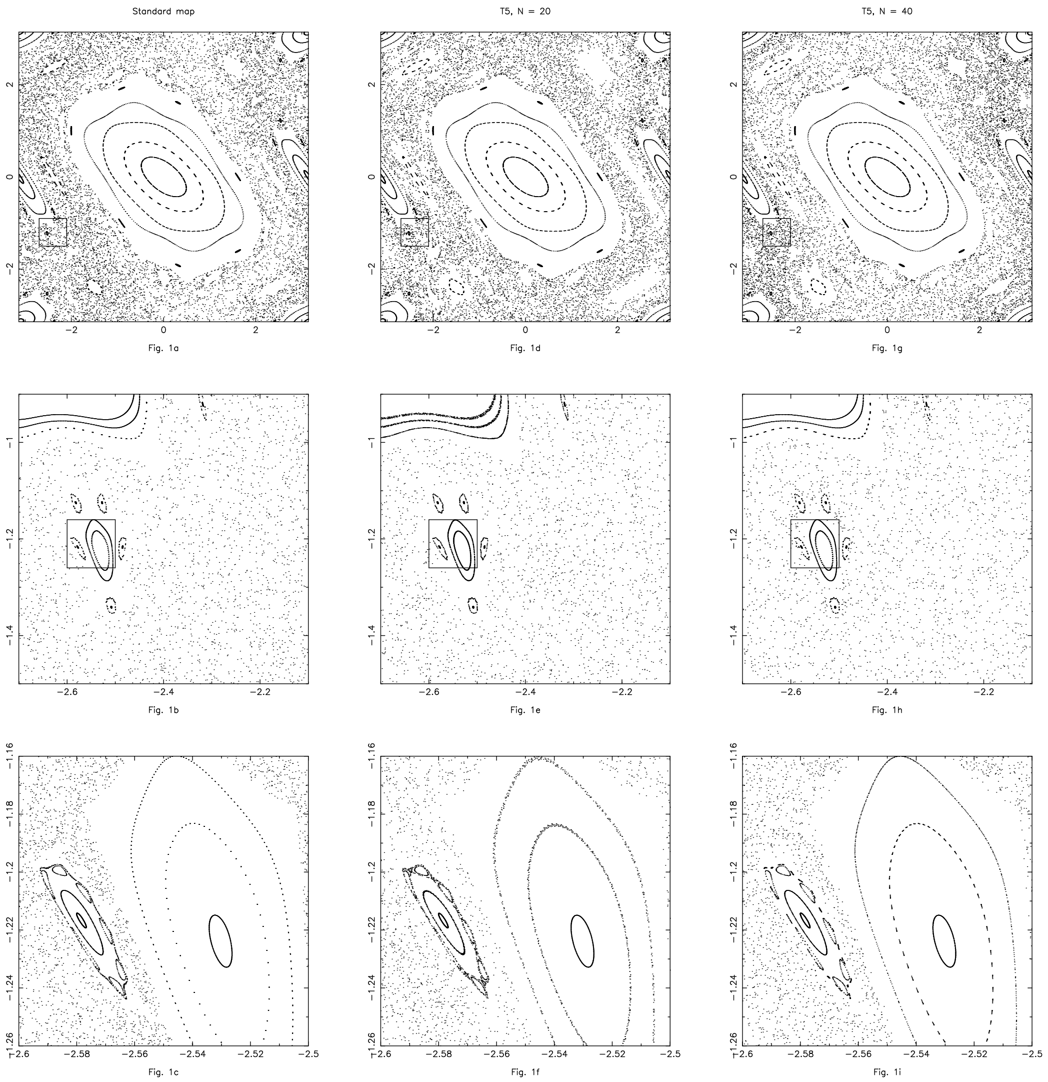

Fig. 1: (a) Standard mapping pictures for $a = -1.3$. (b and c) are enlargements of the small boxes shown in figs. 1a and 1b respectively. (d, e and f) same as figs. 1a,b,c for the synthetic mapping T5 and N=20. (g, h and i) same as figs. 1d,e,f for N=40.

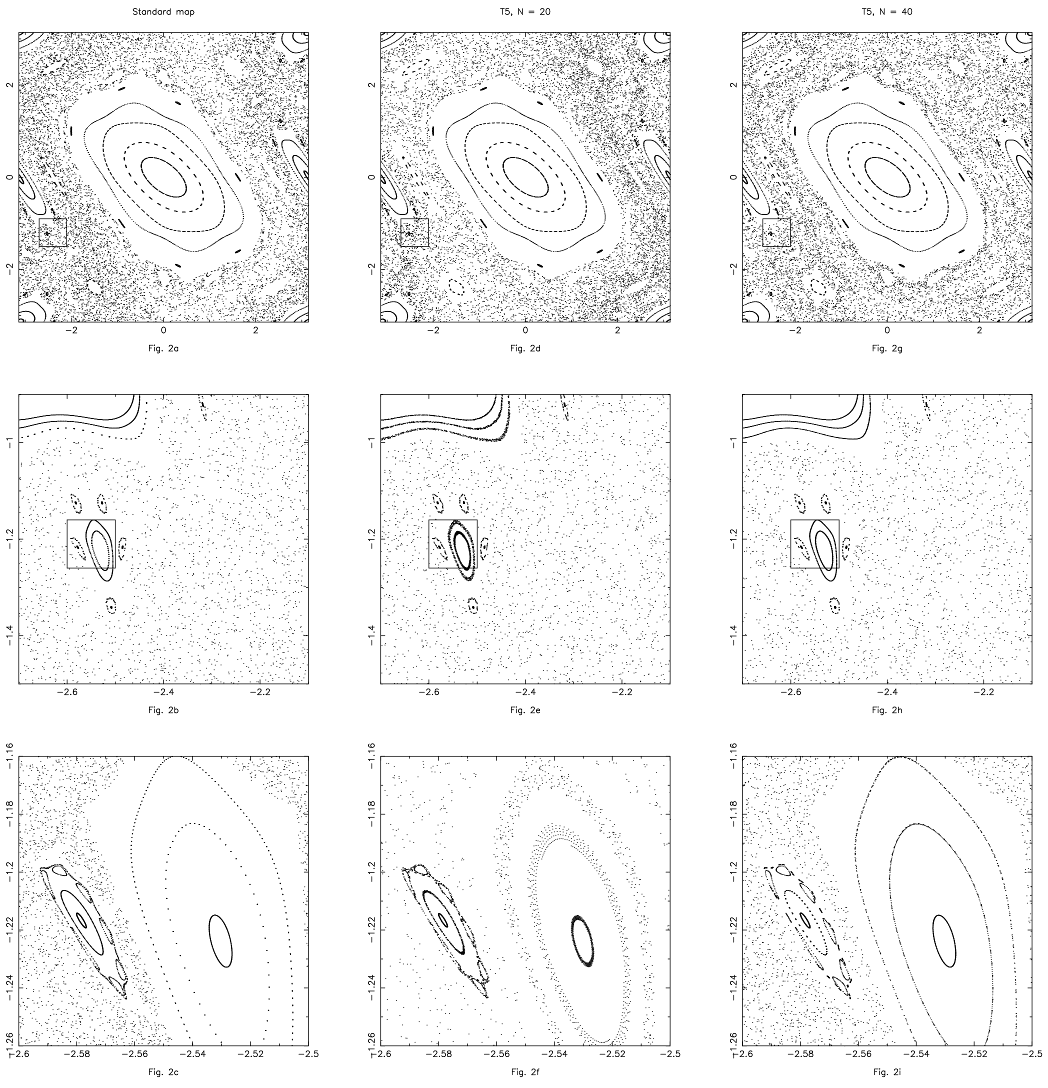

Fig. 2: (a-i) same as figs. 1a-i with the asymmetrical formulae for the T5 maps.

First we used the well-known standard mapping (Froeschle, 1970; Chirikov, 1979; Lichtenberg and Lieberman, 1983):

$$\begin{aligned} x^{(n+1)} &= x^{(n)} + a\sin(x^{(n)} + y^{(n)}) \qquad (\mathrm{mod}\, 2\Pi) \\ y^{(n+1)} &= x^{(n)} + y^{(n)} \qquad (\mathrm{mod}\, 2\Pi). \end{aligned}$$

Fig. 1a shows orbits of the standard mapping for $a = -1.3$. Indeed such a mapping exhibits all the characteristics and well known features of problems with two degrees of freedom such as invariant curves, islands and stochastic zones where the points wander about in a chaotic way. Figs 1b and 1c are magnifications of the small boxes indicated in figs 1a and 1b respectively. At this magnification details like second order islands become evident and the quality of the approximation for the synthetic map is easily visualised. Figs 1g, 1h and 1i correspond respectively to the same orbits and same magnifications as 1a, 1b and 1c for the Taylor interpolation mapping of order $M = 5$ (T5) where the grid is characterized by $N = 40$. We obtain results which look the same as for the original map. For a grid corresponding to $N = 20$ (figs 1d, 1e and 1f), it is interesting to notice the agreement of the details in magnifications e and f. This agreement is remarkable since the dimension of the cell (0.31) is much bigger than the dimension of the smallest islands seen in fig 1f (0.005). Of course the invariant curve of the largest island of 1f shows some thickness which disappears for $N = 40$ but would reappear under further magnification. This phenomenon is due to the fact that synthetic mappings like T5 only conserve areas up to order 6. Let us remark that the computation corresponding to fig. 1 were performed using an extended grid so that we only used the symmetrical interpolation formulae. Since there are cases where one can't cross a given limit, we have tested the asymmetrical interpolation formulae as explained in section 2 (see Appendix A for formulae). Fig. 2 shows the same orbits as fig. 1 for the new formulae. The discrepancy in the sharpness of the invariant curves is particularly obvious in fig. 2f where most of the points are in a region corresponding to the asymmetrical formulae. The problem is less stringent for larger values of N since the portion of phase space needing asymmetrical formulae decreases. Of course for all problems where it is possible, symmetrical formulae should be used. In order to make a more quantitative test of the statistical fine-scaled structure of the orbits resulting from the synthetic mappings we have computed and plotted the Lyapunov Characteristic Number (LCN) (see Benettin et al 1980, Froeschle C, 1984). We consider two orbits starting at P_0 and P'_o and denote by $d = \mathrm{dist}(P_0, P'_0)$, the distance between P_0 and P'_0. After time τ, P_0 is in P_1 and P'_0 in P'_1 and we put $d_1 = \mathrm{dist}(P_1, P'_1)$. By a homothesis of the center P_1 with a ratio d/d_1 we get two new starting points P_1 and P''_1 such that $\mathrm{dist}(P_1, P''_1) = d$ and we iterate the process. It is well known that the quantity

$$\Gamma(n, p, d, \tau) = \frac{1}{n\tau} \sum_{i=1}^{n} \ln(d_i/d) \tag{15}$$

tends to a limit, independent of d and τ, which is the largest LCN as n goes to infinity. We must keep in mind that strictly speaking the LCN's are limiting values as $t \to \infty$; evidently these cannot in practice be computed. We then define the Lyapunov characteristic indicators (LCIs) as the truncated values of the LCNs for a finite time. The variation of $\lambda = \ln(\Gamma)$ with n

for $\tau = 10$ and $d = 10^{-8}$, is shown on fig. 3, for an invariant curve of the Taylor mapping and with the same initial conditions for the different synthetic maps T1, T3, T5 and S3. The grid is such that $N = 100$. For T1 the fit is quite good up to 10^4 iterations. After that the map shows a strong contracting character and looses its area preserving property. The same occurs but for larger n to the spline approximation S3. The Taylor approximations T3 and T5 are better and show the appearance of divergence from the real mapping after 10^6 iterations for T3 and 10^7 for T5. Fig. 4 exhibits the variations of λ as a function of N (coarse graining) for a given value of the LCI, $\Gamma(n, p, d, \tau) = \Gamma(10000, p, 10^{-8}, 10)$. Again the Taylor approximations T3 and T5 show the best fits to the real integrable case. The way λ varies for a cross section on the x-axis at $y_0 = 0$ and $a = -1.3$ is shown as a function of the different mappings (viz. standard map, T1, T3, T5 and S3) in figs. 5a, 5b, 5c for $N = 20$, 50 and 100 respectively. The initial conditions x_0, y_0 are changed along the x-axis ($y_0 = 0$) in steps of 0.1 on the plateaux, and 0.02 at the borders. We again underline the excellence of the fit for the Taylor expansion and also for chaotic orbits the constancy of the values of λ independently of both the coarse graining and the order of the approximation.

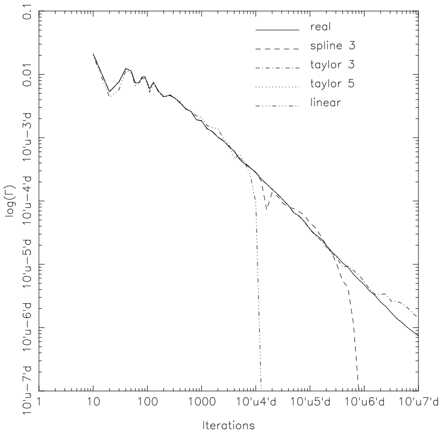

Fig. 3: Variation of the values of the Lyapunov Characteristic Indicators (LCI) for initial conditions corresponding to an invariant curve. The standard map and corresponding synthetic maps are considered.

For more clarity, we consider only the real and T5 mappings for three different values of $N = 20$, 50 and 100 and in fig. 6a we plot λ versus x, as in figs. 5a, 5b, 5c. For $N = 100$, the curves are superimposed and the fit is still very good for $N = 50$. When N is only equal to 20 some slight quantitative differences can be observed but, since the size and location of the stochastic zone remain the same, qualitatively the agreement is excellent. In fig. 6b we present the enlargement of the right hand border of the secondary island which lies to the far left of fig. 6a for $-2.48 \leq x_0 \leq -2.45$ (see region I in fig. 6a). The previous results are confirmed.

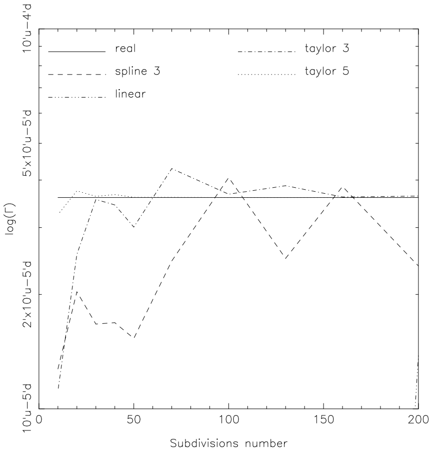

Fig. 4: Variation of the values of the Lyapunov Characteristic Indicator (LCI) computed at 100000 iterations against N which characterises the thinness of the grid for different synthetic maps corresponding to the standard map ($a = -1.3$) and for the same initial conditions ($x_0 = 0.5$, $y_0 = 0$) corresponding to an invariant curve of the standard map.

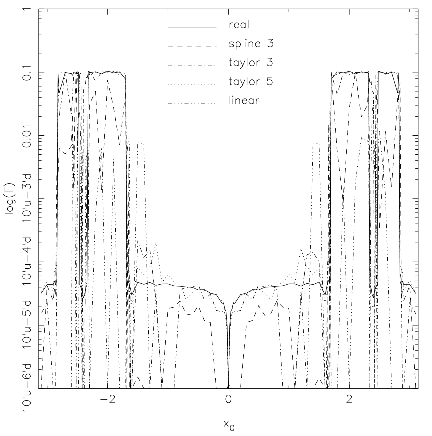

Fig. 5a: Variation along the x-axis of the values of the Lyapunov Characteristic Indicator (LCI) computed at 100000 iterations at $y_0 = 0$ for a value $N = 20$ of the coarse graining parameter.

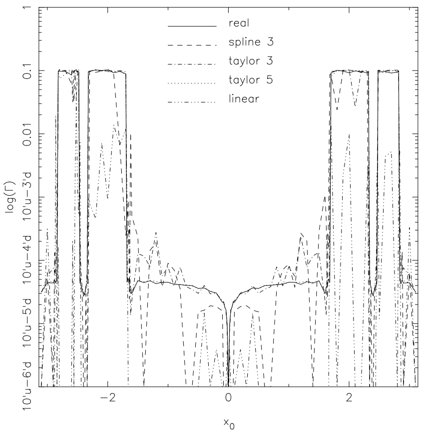

Fig. 5b: Same as fig. 5a for $N = 50$

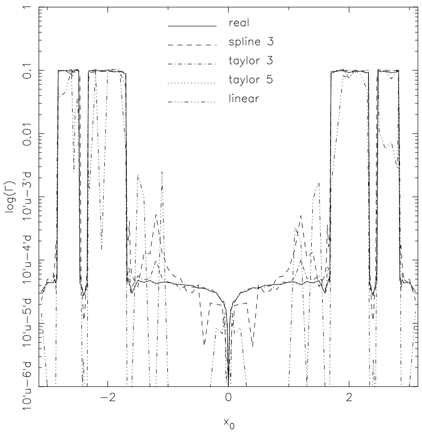

Fig. 5c: Same as fig. 5a for $N = 100$

Finally we have tested the method on a special case of the restricted three body problem for which Duncan et al (1989) have developed a special mapping. Fig. 7a exhibits orbits of the Poincare map taking as surface of section the plane defined by the eccentricity and the mean longitude as polar coordinates, when the particle is in conjonction with the planet (i.e. in the rotating frame, when $y = 0$ and $y' > 0$). In figs. 7b, c, d are plotted the corresponding orbits for synthetic mappings T1, T3, T5 for a grid with $N = 100$. If the linear mapping T1 shows only poor qualitative similarities with the Poincare map, the T3 map correctly reproduces the locations, shapes and sizes of zones of regular orbits. Of course the T5 map is even better. It should be noted that in order to obtain the same accuracy we needed to use a smaller grid size (i.e. more points) than for the standard map since the functions which have to be interpolated are less regular. In this case, we needed about 80 minutes to compute the Poincare map by integrating the equations of motion (fig. 7a) and only 2 seconds for T5 (fig. 7d). However one has to allow for the time needed to compute the grid.

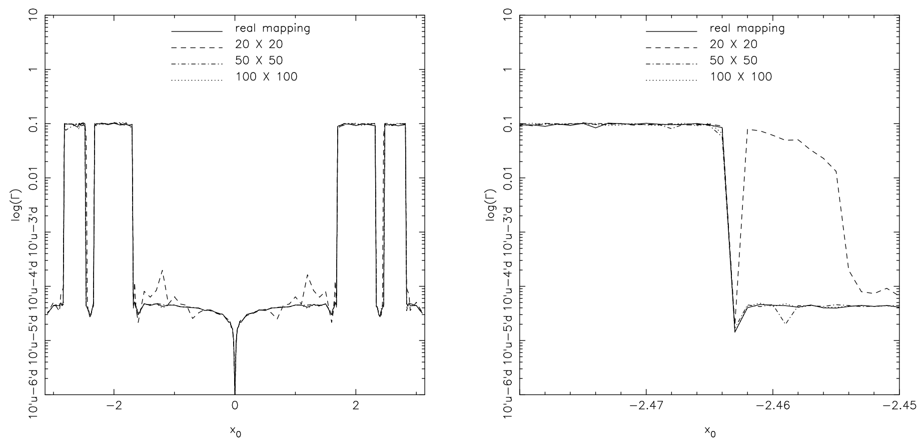

Fig. 6: (a) same as fig. 5 for the synthetic mapping T5 and for different values of the parameter grid. (b) enlargement of the border of a secondary island (zone I) for $-2.48 \leq x_0 \leq -2.45$.

Let us remark that the same accuracy as that obtained by the T5 map can be obtained even with the T1 map by drastically decreasing the size of the grid cells (i.e. by increasing N). Actually for such an increase in the number of vertices, the price to pay is very small since the additional Poincare return map values at the vertices can be computed using the more precise mapping T5. Figs. 7e,f show the T1 and T3 mappings for a grid with $N = 400$, where 15/16 of the N^2 map values at the vertices have been computed using T5 through the already computed grid with $N = 100$. The time needed to compute the 10000 points of the initial grid is about 5 hours 40 minutes and it took only 70 seconds to compute the 150000 news points. In this case T5 is about 300 times faster than the integration. And when looking at the long term evolution, one will still save time if one wants to iterate for 200000 or more steps, since T1 is about 16 times faster than T5. Indeed the accuracy of T1 is greatly improved. Of course the same holds for T3. This combination of the order of interpolation and of different coarse graining, i.e. of different mappings appears very promising for four dimensional mappings where the computational time of T5 is far from negligible as shown in section 2.3

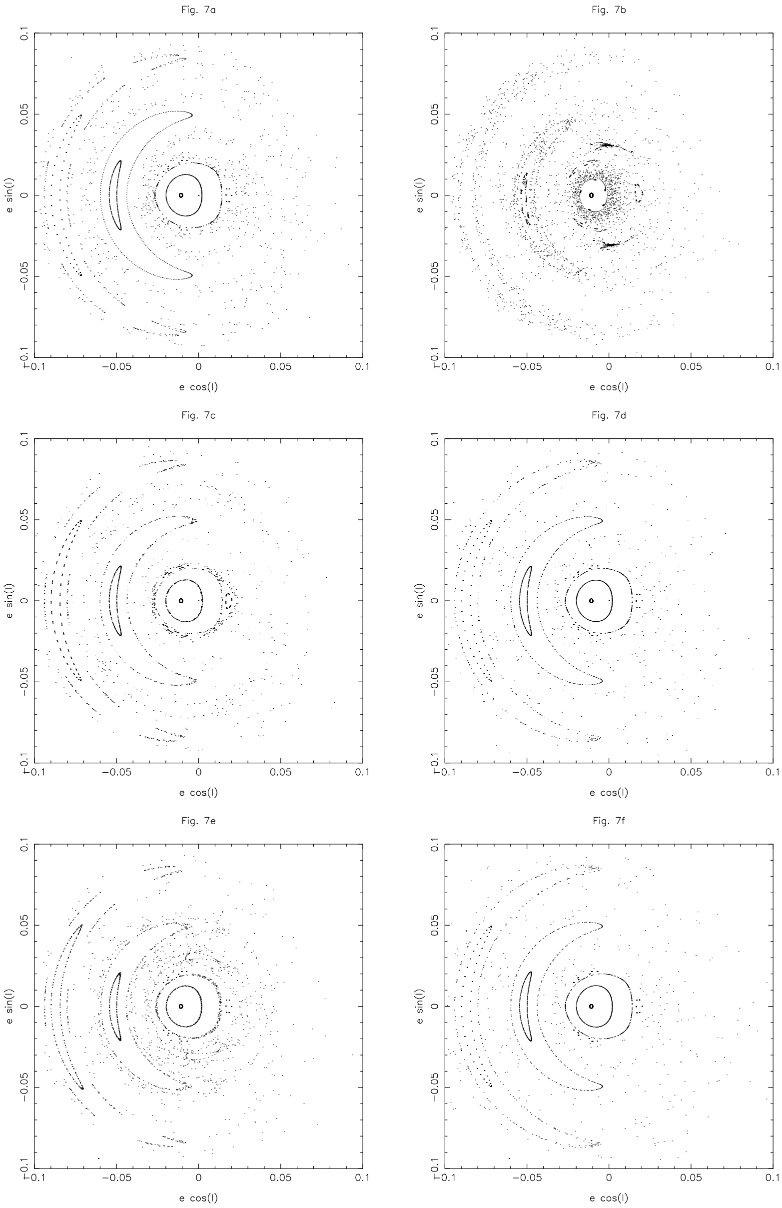

Fig. 7: (a) Trajectories of the Poincaré map of the restricted three body problem, in the plane (eccentricity, mean longitude) (polar coordinates) at conjonction with the planet, for the Neptune - Sun mass ratio $m/M_{\odot} = 5.178\, 10^{-5}$ and Jacobi constant 3.0080694. (b, c and d) same as fig. 7a for the synthetic maps T1, T3 and T5. (e and f) Same as fig. 7b,c for a grid with $N = 400$ obtained with T5.

4 Conclusion

Synthetic maps appear to be valuable tools for celestial mechanics. However for problems with more than two degrees of freedom the situation is less straightforward. The number of operations required for the Taylor approxmation increases drastically with the dimension of the surface of section. Of course as shown above a lower order map can be used by decreasing the grid size but a second difficulty is the task of storing and recalling the values of the computed images at the vertices. In any case some compromises have to be made between the number of cells and the order of the polynomial approximation. All of these problems will be developed in a forthcoming paper.

Appendix A

The interpolating formula for the border cells are of the same form as before:

$$f(x) = \sum \Phi_n(\frac{x - x'}{h}) f(x_{i+n}). \tag{16}$$

We first give the formulae for mapping T5. For $x_0 \leq x \leq x_1$, the $\Phi_n(X)$ are:

$$\begin{aligned}
\Phi_0(X) &= \frac{1}{3840}[945 - 3378X + 3800X^2 \\
&\quad -1840X^3 + 400X^4 - 32X^5], \\
\Phi_1(X) &= \frac{1}{3840}[4725 + 2010X - 10760X^2 \\
&\quad +7280X^3 - 1840X^4 + 160X^5], \\
\Phi_2(X) &= \frac{1}{3840}[-3150 + 2860X + 11760X^2 \\
&\quad -11360X^3 + 3360X^4 - 320X^5], \\
\Phi_3(X) &= \frac{1}{3840}[1890 - 2220X - 6800X^2 \\
&\quad +8800X^3 - 3040X^4 + 320X^5], \\
\Phi_4(X) &= \frac{1}{3840}[-675 + 870X + 2360X^2 \\
&\quad -3440X^3 + 1360X^4 - 160X^5], \\
\Phi_5(X) &= \frac{1}{3840}[105 - 142X - 360X^2 \\
&\quad +560X^3 - 240X^4 + 32X^5].
\end{aligned} \tag{17}$$

For $x_1 \leq x \leq x_2$, we have:

$$
\begin{aligned}
\Phi_{-1}(X) &= \frac{1}{3840}[-105 + 142X + 360X^2 \\
&\quad -560X^3 + 240X^4 - 32X^5], \\
\Phi_0(X) &= \frac{1}{3840}[1575 - 4230X + 1640X^2 \\
&\quad +1520X^3 - 1030X^4 + 160X^5], \\
\Phi_1(X) &= \frac{1}{3840}[3150 + 4140X - 5360X^2 \\
&\quad -1120X^3 + 1760X^4 - 320X^5], \\
\Phi_2(X) &= \frac{1}{3840}[-1050 + 20X + 4560X^2 \\
&\quad -160X^3 - 1440X^4 + 320X^5], \\
\Phi_3(X) &= \frac{1}{3840}[315 - 90X - 1400X^2 \\
&\quad +400X^3 + 560X^4 - 160X^5], \\
\Phi_4(X) &= \frac{1}{3840}[-45 + 18X + 200X^2 \\
&\quad -80X^3 - 80X^4 + 32X^5].
\end{aligned}
\tag{18}
$$

By symmetry, we have for $x_{n-2} \leq x \leq x_{n-1}$:

$$
\begin{aligned}
\Phi_{-4}(X) &= \frac{1}{3840}[-45 - 18X + 200X^2 \\
&\quad +80X^3 - 80X^4 - 32X^5], \\
\Phi_{-3}(X) &= \frac{1}{3840}[315 + 90X - 1400X^2 \\
&\quad -400X^3 + 560X^4 + 160X^5], \\
\Phi_{-2}(X) &= \frac{1}{3840}[-1050 - 20X + 4560X^2 \\
&\quad +160X^3 - 1440X^4 - 320X^5], \\
\Phi_{-1}(X) &= \frac{1}{3840}[3150 - 4140X - 5360X^2 \\
&\quad +1120X^3 + 1760X^4 + 320X^5], \\
\Phi_0(X) &= \frac{1}{3840}[1575 + 4230X + 1640X^2
\end{aligned}
\tag{19}
$$

$$
\begin{aligned}
& -1520X^3 - 1030X^4 - 160X^5], \\
\Phi_1(X) &= \frac{1}{3840}[-105 - 142X + 360X^2 \\
& +560X^3 + 240X^4 + 32X^5].
\end{aligned}
$$

Finally, for $x_{n-1} \leq x \leq x_n$, the formulae are as follow:

$$
\begin{aligned}
\Phi_{-5}(X) &= \frac{1}{3840}[105 + 142X - 360X^2 \\
& -560X^3 - 240X^4 - 32X^5], \\
\Phi_{-4}(X) &= \frac{1}{3840}[-675 - 870X + 2360X^2 \\
& +3440X^3 + 1360X^4 + 160X^5], \\
\Phi_{-3}(X) &= \frac{1}{3840}[1890 + 2220X - 6800X^2 \\
& -8800X^3 - 3040X^4 - 320X^5], \\
\Phi_{-2}(X) &= \frac{1}{3840}[-3150 - 2860X + 11760X^2 \\
& +11360X^3 + 3360X^4 + 320X^5], \\
\Phi_{-1}(X) &= \frac{1}{3840}[4725 - 2010X - 10760X^2 \\
& -7280X^3 - 1840X^4 - 160X^5], \\
\Phi_0(X) &= \frac{1}{3840}[945 + 3378X + 3800X^2 \\
& +1840X^3 + 400X^4 + 32X^5].
\end{aligned}
\tag{20}
$$

We now give the formulae for mapping T3. Firstly for $x_0 \leq x \leq x_1$:

$$
\begin{aligned}
\Phi_0(X) &= \frac{1}{48}\left[15 - 46X + 36X^2 - 8X^3\right], \\
\Phi_1(X) &= \frac{1}{48}\left[45 + 42X - 84X^2 + 24X^3\right], \\
\Phi_2(X) &= \frac{1}{48}\left[-15 + 6X + 60X^2 - 24X^3\right], \\
\Phi_3(X) &= \frac{1}{48}\left[3 - 2X - 12X^2 + 8X^3\right].
\end{aligned}
\tag{21}
$$

And for $x_{n-1} \leq x \leq x_n$:

$$
\Phi_{-3}(X) = \frac{1}{48}\left[3 + 2X - 12X^2 - 8X^3\right],
$$

$$
\begin{aligned}
\Phi_{-2}(X) &= \frac{1}{48}\left[-15 - 6X + 60X^2 + 24X^3\right], \\
\Phi_{-1}(X) &= \frac{1}{48}\left[45 - 42X - 84X^2 - 24X^3\right], \\
\Phi_{0}(X) &= \frac{1}{48}\left[15 + 46X + 36X^2 + 8X^3\right].
\end{aligned} \tag{22}
$$

References

[1] ARNOLD, V.I., 1976. in *Méthodes mathématiques de la mécanique céleste,* Eds. de Moscou,

[2] BAILLE, PH., & FROESCHLE, C., 1989. Astron. Astrophys., in press,

[3] BENETTIN, G.L., GIORGILLI, A., & STRELCYN, J.M., 1980. Meccanica **15**, p. 10.

[4] CHIRIKOV, B.V., 1979. *Phys.Rev..* **52**, p. 263.

[5] DUNCAN, M., QUINN, T., & TREMAINE S., 1989. Icarus **82**, p. 402.

[6] FROESCHLE, C., 1970. Astron. Astrophys. **9**, p. 15.

[7] FROESCHLE, C., 1984. Numéro special du Journal de Mécanique théorique et appliquée p. 101.

[8] FROESCHLÉ, C., & RICKMAN, H., 1980. *Astron.Astophys..* **82**, p. 183.

[9] FROESCHLE, C., & SCHOLL, H., 1981. Astron. Astrophys. **93**, p. 62.

[10] HADJIDEMETRIOU, J.D., 1986. Journal of applied Mathematics and Physic **37**, p. 776.

[11] HÉNON, M., 1981. in *Cours des Houches,* **XXXVI**, North Holland, Amsterdam, p. 57.

[12] HÉNON, M., & PETIT, J.M., 1986. Celestial Mechanics **38**, p. 67.

[13] LICHTENBERG, A.J., & LIEBERMAN, M.A., 1983. in *Regular and Stochastic motion,* Springer Verlag,

[14] MILANI, A., CARPINO, M.,HAHN, G., & NOBILI, A.M., 1989. Icarus **78**, p. 212.

[15] MURRAY, C.D., 1986. Icarus **65**, p. 70.

[16] Petrosky, T.Y., & Broucke, R., 1988. *CelestialMechanics.* **42**, p. 53.

[17] Rickman, H., & Vaghi, S., 1976. Astron. Astrophys. **51**, p. 327.

[18] Sagdeev, R.Z., & Zaslavsky, G.M., 1987. Il nuovo cimento **97b**, 2.

[19] Schubart, J., 1968. Astron. J. **73**, p. 99.

[20] Sidlichovsky, M., & Melenda, B., 1986. Bull. Astron. Inst. Czechosl. **37**, p. 65.

[21] Varosi, F., Grebogi, C., & Yorke, J.A., 1987. Physics Letters A **124**, p. 59.

[22] Wisdom, J., 1982. Astron. J. **87**, p. 577.